Published in final edited form as:

Sci Signal. 2024 June 11; 17(840): eadn8376. doi:10.1126/scisignal.adn8376.

Slow proliferation of BAP1-deficient uveal melanoma cells is associated with reduced S6 signaling and resistance to nutrient stress

Vivian Chua[1,2,3], **Melisa Lopez-Anton**[4], **Mizue Terai**[5], **Ryota Tanaka**[5], **Usman Baqai**[1], **Timothy J. Purwin**[1], **Jelan I. Haj**[1], **Francis J. Waltrich Jr.**[1], **Isabella Trachtenberg**[1], **Kristine Luo**[1], **Rohith Tudi**[1], **Angela Jeon**[1], **Anna Han**[6], **Inna Chervoneva**[7], **Michael A. Davies**[8], **Julio A. Aguirre-Ghiso**[9,10,11,12,13], **Takami Sato**[5], **Andrew E. Aplin**[1,14,*]

[1]Department of Pharmacology, Physiology, and Cancer Biology, Thomas Jefferson University, Philadelphia, PA 19107 USA.

[2]School of Medical and Health Sciences, Edith Cowan University, Joondalup, Perth, WA 6027 Australia.

[3]Centre for Precision Health, Edith Cowan University, Joondalup, Perth, WA 6027 Australia.

[4]Division of Hematology and Oncology, Department of Medicine, Department of Otolaryngology, Department of Oncological Sciences, Black Family Stem Cell Institute, Tisch Cancer Institute, Icahn School of Medicine at Mount Sinai, New York, NY 10029 USA.

[5]Department of Medical Oncology, Thomas Jefferson University, Philadelphia, PA 19107 USA.

[6]Department of Food Science and Human Nutrition, Jeonbuk National University, Jeonju, Jeollabuk-do 54896, Republic of Korea.

[7]Division of Biostatistics, Department of Pharmacology and Experimental Therapeutics, Thomas Jefferson University, Philadelphia, PA 19107 USA.

[8]Department of Melanoma Medical Oncology, The University of Texas MD Anderson Cancer Center, Houston, TX 77030 USA.

[9]Department of Cell Biology, Albert Einstein College of Medicine, Bronx, NY 10461 USA.

[10]Cancer Dormancy and Tumor Microenvironment Institute, Albert Einstein College of Medicine, Bronx, NY 10461 USA.

[*]Corresponding author. Andrew.Aplin@Jefferson.edu.

Author contributions: Conceptualization: V.C. and A.E.A. Methodology: V.C., M.L-A., M.T., and R.Tanaka. Investigation: V.C., M.L-A., M.T., R.Tanaka, U.B., T.J.P., J.I.H., F.J.W., I.T., K.L., R.Tudi, A.J., and A.H. Visualization: V.C., M.L-A., M.T., R.Tanaka, T.J.P., J.I.H., F.J.W., I.T., K.L., R.Tudi, A.J., A.H., and I.C. Funding acquisition: V.C., M.A.D., and A.E.A. Project administration: V.C., T.S., and A.E.A. Supervision: J.A.A-G., T.S., and A.E.A. Writing: Original draft, V.C.; review and editing: V.C., M.L.A., M.T., U.B., A.H., M.A.D., J.A.A-G., T.S., and A.E.A.

Competing interests: A.E.A. has ownership interest in patent number 9880150 and has a pending patent, PCT/US22/76492. M.A.D. has been a consultant to Roche/Genentech, Array, Pfizer, Novartis, BMS, GSK, Sanofi-Aventis, Vaccinex, Apexigen, Eisai, Iovance, and ABM Therapeutics, and he has been the PI of research grants to MD Anderson by Roche/Genentech, GSK, Sanofi-Aventis, Merck, Myriad, Oncothyreon, ABM Therapeutics, and LEAD Pharma. J.A.A-G. is a scientific co-founder, scientific advisory board member and equity owner in HiberCell and receives financial compensation as a consultant for HiberCell, a Mount Sinai spin-off company focused on the research and development of therapeutics that prevent or delay the recurrence of cancer. All other authors declare that they have no potential conflicts of interest.

[11]Montefiore Einstein Cancer Center, Albert Einstein College of Medicine, Bronx, NY 10461 USA.

[12]Gruss-Lipper Biophotonics Center, Albert Einstein College of Medicine, Bronx, NY 10461 USA.

[13]Ruth L. and David S. Gottesman Institute for Stem Cell Research and Regenerative Medicine, Albert Einstein College of Medicine, Bronx, NY 10461 USA.

[14]Sidney Kimmel Cancer Center, Thomas Jefferson University, Philadelphia, PA 19107 USA.

Abstract

Uveal melanoma (UM) is the deadliest form of eye cancer in adults. Inactivating mutations and/or loss of expression of the gene encoding BRCA1-associated protein 1 (BAP1) in UM tumors are associated with an increased risk of metastasis. To investigate the mechanisms underlying this risk, we explored the functional consequences of BAP1 deficiency. UM cell lines expressing mutant BAP1 grew more slowly than those expressing wild-type BAP1 in culture and in vivo. The ability of BAP1 reconstitution to restore cell proliferation in BAP1-deficient cells required its deubiquitylase activity. Proteomic analysis showed that BAP1-deficient cells had decreased phosphorylation of ribosomal S6 and its upstream regulator, p70S6K1, compared to both wild-type and BAP1 reconstituted cells. In turn, expression of p70S6K1 increased S6 phosphorylation and proliferation of BAP1-deficient UM cells. Consistent with these findings, BAP1 mutant primary UM tumors expressed lower amounts of p70S6K1 target genes, and S6 phosphorylation was descreased in BAP1-mutant patient-derived xenografts (PDXs), which grew more slowly than wild-type PDXs in the liver (the main metastatic site of UM) in mice. BAP1-deficient UM cells were also more resistant to amino acid starvation, which was associated with diminished phosphorylation of S6. These studies demonstrate that BAP1 deficiency slows the proliferation of UM cells through regulation of S6 phosphorylation. These characteristics may be associated with metastasis by ensuring survival during amino acid starvation.

Introduction

Uveal melanoma (UM) is diagnosed in approximately 2,500 adults annually in the US (1). Approximately 50% of patients develop metastasis, mainly in the liver, even years after successful treatment of primary tumors by either radiation plaque therapy or enucleation (2). Metastases can develop several months to 20 years after primary tumor treatment, suggesting that UM cells disseminate early from the primary site and “seed” at a secondary organ site. Despite effective treatment of primary UM tumors, metastatic UM responds poorly to molecularly targeted therapies and immune checkpoint blockade (3, 4). Median survival in patients is 5 to 18 months after diagnosis of metastasis (5). Thus, there is an urgent need to identify the mechanisms promoting metastasis of UM such that novel therapeutic strategies can be developed.

The most common mutations in UM occur in *GNAQ* and *GNA11*, which encode the G proteins $G\alpha_q$ (guanine nucleotide-binding protein subunit alpha q) and $G\alpha_{11}$, respectively. These mutations abolish their ability to hydrolyze GTP to GDP, resulting in constitutive activation of downstream signaling that includes mitogen-activated protein kinase (MAPK) pathways. Activating *GNAQ/11* mutations are initiating events in UM and are major drivers

of UM development (6). Together with *CYSLTR2* and *PLCB4* mutations, they occur in >95% of UM in a mutually exclusive manner. Chromosomal abnormalities and secondary mutations in genes encoding BRCA1-associated protein 1 (*BAP1*), splicing factor 3B subunit 1 (*SF3B1*), and eukaryotic translation initiation factor 1A X-linked (*EIF1AX*) are associated with metastasis risk and prognosis in UM patients—tumors with monosomy 3, gain of chromosome 8q, and/or alterations in *BAP1* have an increased risk of metastasis, whereas mutations in *EIF1AX* and *SF3B1* are associated with better prognosis (7, 8).

BAP1 is a tumor suppressor gene located on chromosome 3p21.1. *BAP1* encodes a deubiquitylating (DUB) enzyme that removes mono-ubiquitin from proteins such as histones (9). Deubiquitylation leads to the stabilization of histones and transcriptional regulation of genes that control DNA damage repair, cell proliferation, and cell differentiation. Monosomy 3 is a marker of poor prognosis in UM and often co-occurs with *BAP1* inactivating mutations. Losing one allele of chromosome 3 likely complements *BAP1* mutations to cause loss of BAP1 function. *BAP1* mutations have been reported in 30–40% of UM cases and the majority (~85%) of these cases were categorized as Class 2, a subset of UM with an increased risk of metastasis (7, 10). Notably, knockdown of *BAP1* does not increase UM cell proliferation, migration, or invasion in vitro, or metastasis in vivo (11). Further, transient knockdown of *BAP1* in UM cell lines inhibits cell proliferation and promotes cell cycle arrest (11). Determining the mechanisms that mediate these effects of BAP1 loss could improve our understanding of its role in the pathogenesis of UM and may lead to new and more effective therapeutic strategies for this disease.

Here, we functionally evaluated the role and associations of *BAP1* in UM cell lines, xenografts, and clinical samples. We found that loss of BAP1 alters UM cell proliferation and signaling that may support the survival of UM cells during metastatic dissemination.

Results

BAP1 loss is associated with slow proliferation of UM cells

Loss of expression and/or function of BAP1 is correlated with poor patient survival and a high likelihood of UM progression (12). However, knockdown of *BAP1* expression has been reported to inhibit UM cell proliferation in vitro and to induce cell cycle arrest (11). Consistently, we found that the BAP1-deficient UM cell lines MP46, MP65, and MP38 proliferated more slowly than the *BAP1* wild-type (WT) UM cell lines, 92.1 and MM66 (Fig. 1, A and B). To test the role of BAP1 in cell growth, we modulated BAP1 expression in the UM cell lines. siRNA-mediated knockdown of BAP1 diminished 92.1 cell viability (Fig. 1, C and D). As a complementary approach, we re-introduced WT or DUB-mutant (C91A or C91G) forms of BAP1 into BAP1-deficient MP65 and MP46 cells by lentiviral transduction (Fig. 1, E and F). C91A and C91G are alterations in amino acid position 91 of BAP1 from cysteine to alanine or glycine, respectively. This position is located in the BAP1 domain that controls its DUB activity. Re-expression of BAP1 WT but not BAP1 C91A or BAP1 C91G increased MP65 and MP46 cell proliferation in vitro (Fig. 1, G to L), indicating that the DUB function of BAP1 is involved in regulating UM cell proliferation.

Next, we investigated the effect of BAP1 status on UM cell proliferation in vivo and in 3D cultures. Subcutaneous xenograft tumors in NSG mice were larger in mice injected with *BAP1* WT re-expressing MP65 and MP46 cells compared to mice injected with the parental cell lines by week 9 (Fig. 2, A and B). For 3D culture experiments, cells were seeded as single cells in Matrigel. On day 4, there were more multi-cell clusters and fewer single cells for BAP1 re-expressing MP65 and MP46 cells compared to the parental cell lines (Fig. 2, C and D). The majority (~77%) of MP65 were single cells. Altogether, our results indicated that the loss of BAP1 leads to slower proliferation in UM cells in vitro and in vivo.

BAP1 re-expression increases the phosphorylation of ribosomal S6

We performed RPPA analysis to identify potential mechanisms underlying the difference in proliferation between BAP1-deficient and BAP1-proficient UM cells. RPPA is a high-throughput analysis of expression of 492 proteins and phospho-proteins. We determined the fold change in levels of proteins associated with cell proliferation between *BAP1* WT UM cell lines (n=6) and BAP1-deficient UM cell lines (n=6), and between *BAP1* WT re-expressing MP65 cells and parental MP65 cells, growing in vitro (table S1). We found that the levels of pS6 at $Ser^{235/236}$ and $Ser^{240/244}$ were higher in both *BAP1* WT and BAP1 re-expressing cells (Fig. 3A). In the UM cell line panel, pS6 was significantly lower in BAP1-deficient cells than in *BAP1* WT cells although there is heterogeneity in pS6 (Fig. 3B). As with all arrays, these RPPA data will need to be validated with optimized conditions. These results were confirmed by Western blotting, which showed low to undetectable levels of pS6 in all BAP1-deficient UM cells (Fig. 3C). *BAP1* WT cells exhibited either low (OMM1.3, UM002B, and UM004) or high (UM001, 92.1, and MM66) levels of pS6 (Fig. 3, C to E). These findings indicated that heterogeneity in pS6 levels exists, but overall pS6 levels are higher in *BAP1* WT than in BAP1-deficient UM cells.

To determine whether changes in pS6 were dependent on BAP1 expression and/or function, we measured pS6 levels in BAP1 transduced cells. Expression of BAP1 WT increased levels of pS6 and phosphorylation of its upstream regulator, p70S6K1, in MP65 and MP46 cells (Fig. 3F and fig. S1). Expression of DUB-mutant BAP1 (C91A) did not increase pS6 or pp70S6K1 levels compared to those in parental cells, indicating that the DUB activity of BAP1 regulates phosphorylation of S6 and p70S6K1. We observed only a slight increase in phosphorylated mTOR (p-mTOR) which is canonically upstream of pS6 and phospho-p70S6K1 (p-p70S6K1) (Fig. 3F and fig. S1). Consistent with data from 2D cultures, the prevalence of pS6-positive cells was higher in MP65 and MP46 cells exogenously expressing BAP1 compared to the BAP1-deficient parental cells when grown as 3D cultures in Matrigel (Fig. 3G). These findings showed that BAP1 regulates pS6 and p-p70S6K1 levels.

AMPK promotes low pS6 which is associated with slow proliferation of BAP1-deficient UM cells

To elucidate the mechanism mediating BAP1 regulation of pS6, we examined RPPA data for differentially expressed proteins between BAP1-deficient and BAP1 transduced cells that are associated with the mTOR/S6 pathway. These proteins included the kinases Aurora-A, AKT, and AMP-dependent kinase (AMPK) (Fig. 4A) (13–15). We were not able to verify

alterations in Aurora-A and AKT by Western blotting but observed increased levels of phosphorylated AMPK (pAMPK) in BAP1-deficient MP46 and MP65 cells compared to BAP1-reexpressing counterparts, a finding that is consistent with a previous study (Fig. 4B and fig. S2) (16). The AMPK pathway has been shown to inhibit mTOR signaling in other cell types (17, 18). To determine whether AMPK inhibits mTOR and S6 in UM cells, *BAP1* WT cell lines 92.1 and MM66 were treated with an AMPK activator, metformin. Activation of AMPK decreased pS6, p-p70S6K1, and p-mTOR levels (Fig. 4C and fig. S3).

Slow proliferation in BAP1-deficient UM cells is associated with low pS6

Phosphorylation of S6 promotes protein translation and cell proliferation (19); hence, we determined whether there is an association between the slow proliferation of BAP1-deficient UM cells and low pS6 levels. We investigated the effect of inducing pS6 on the proliferation of MP65 and MP46 (BAP1-deficient UM cell lines). To induce pS6, cells were transduced with either the active (S6K1 ΔCt) or wild-type form of p70S6K1 (S6K1 WT). MP65 cells transduced with S6K1 ΔCt had higher levels of pS6 levels and enhanced cell proliferation in 2D culture compared to MP65 parental cells (Fig. 4, D and E). We successfully transduced S6K1 WT but not S6K1 ΔCt in MP46. Similar to MP65 cells, MP46 cells had higher pS6 levels after transduction with S6K1 WT (Fig. 4F). MP46 S6K1 WT cells were also more confluent than parental cells 3 days after cells were plated at the same seeding density (Fig. 4G). These results indicated that inducing pS6 is sufficient to promote the proliferation of BAP1-deficient UM cells.

pS6 and p70S6K1 target genes are differentially expressed in BAP1-deficient and BAP1-proficient UM patient tumors

We investigated whether our pre-clinical data were consistent with patient tumor data in publicly available datasets. pS6 levels were analyzed in RPPA data from The Cancer Genome Atlas (TCGA) UM dataset (n=12 primary tumors). BAP1-deficient samples were identified based on BAP1 protein expression and the presence of *BAP1* mutations or *BAP1* copy number loss. However, there were no marked differences in pS6 levels between BAP1-deficient and WT tumors (fig. S4). It is possible that the presence of other non-cancer cell types in TCGA samples may mask pS6 levels in tumor cells (20). Hence, we analyzed single cell RNA sequencing data from primary UM tumors and determined changes in ribosomal biogenesis genes regulated by S6K1 selectively in tumor cells as S6K1 is upstream of S6 (21). The ribosomal biogenesis genes included small (RPS) and large (RPL) ribosomal proteins (21). The average mRNA expression of each gene per tumor was determined. The average expression of the *RPS* and *RPL* genes were significantly higher in the *BAP1* WT tumors (Fig. 5A). The mRNA levels of small ribosomal proteins (*RPS*; n=15) and large ribosomal proteins (*RPL*; n=7), except for *RPS10*, *RPS11*, *RPS17*, and *RPL31*, were higher in *BAP1* WT compared to BAP1-deficient tumors (fig. S5). These results indicated that S6K1-regulated transcripts are lower in *BAP1* mutant UM compared to *BAP1* WT UM.

We also determined pS6 levels in liver metastases from UM patients. BAP1 status in these specimens was determined by staining the tissues for BAP1 protein. UMT205B, which had the highest intensity of BAP1 staining, expressed higher levels of pS6 ($Ser^{235/236}$) and the Ki-67 proliferative marker compared to the other two specimens (Fig. 5, B and C). UMT-18–

8-2 and UMT-21–12A had lower staining for BAP1 than did UMT205B and expressed reduced levels of pS6 and Ki-67 (Fig. 5, B and C). These patient-based data support that BAP1 deficiency in UM is associated with lower abundance of pS6.

BAP1 mutant PDX models proliferate slower in vivo

We investigated the effects of BAP1 status on UM proliferation and pS6 in PDX models generated from UM liver metastases (table S2). PDXs maintain the genetic and histological characteristics of patient tumors and can be implanted and grown in mice livers, providing an important model for studying the effects of BAP1 in UM. Consistent with our analysis of clinical samples, pS6 levels were lower in *BAP1* mutant PDX UM models compared to those in *BAP1* WT PDXs (Fig. 6A). Three PDXs were implanted hepatically in NSG mice, and tumor growth was monitored by CT scans. The *BAP1* mutant PDXs, PDX1904 and PDX1905, grew more slowly than the *BAP1* WT PDX, PDX1901 (Fig. 6, B and C). At the final time point, tumors were excised from mouse livers and stained for pS6 and Ki-67. The *BAP1* mutant PDXs expressed lower levels of Ki-67 compared to PDX1901 (*BAP1* WT) (Fig. 6, D to F). PDX1901 (*BAP1* WT) exhibited the most pS6 staining, followed by PDX1904 and PDX1905, which had minimal pS6 staining. Interestingly, pS6 levels in PDX1904 (*BAP1* mutant) were only slightly lower compared to PDX1901 (*BAP1* WT). This is consistent with our in vitro data, which identified heterogeneity in pS6 levels among UM cell lines. Overall, our findings show that whilst there is heterogeneity in pS6 levels in UM cell lines and patient tumor specimens, BAP1 deficiency leads to slower proliferation of UM and a decrease in pS6 levels.

BAP1-deficient UM cells survive better under amino acid starvation

BAP1-deficiency is associated with elevated risks of metastasis of UM in patients, hence we hypothesized that low pS6 and slow proliferation may be promoting processes that support metastasis such as survival under stress. Because S6 is involved in protein translation and response to amino acids, we investigated the effects of amino acid starvation on the viability of BAP1-deficient and *BAP1* WT cells. We found that BAP1-deficient cells, MP38 and MP65, survived better when incubated in amino-acid free culture media compared to *BAP1* WT cells, 92.1 and MM66 and that this resistance in MP65 cells was impaired by ectopic expression of BAP1 (Fig. 7, A to D). Furthermore, MP65 cells expressing active S6K1 ΔCt, were significantly growth inhibited by amino acid starvation compared to MP65 parental cells (Fig. 7, C and D). These findings indicate that the slow proliferation of BAP1-deficient UM cells and low pS6 levels are associated with resistance to amino acid starvation in UM cells.

Discussion

Metastatic UM is associated with frequent copy number loss and/or inactivating mutations in *BAP1*. Understanding the effect of BAP1 status on UM may lead to better treatment strategies for metastatic UM. In this study, we found that BAP1 deficiency leads to slow proliferation of UM cells. Expression of *BAP1* WT in BAP1-deficient UM cells increased cell proliferation in 2D and 3D cultures as well as in vivo. BAP1-deficient UM cells expressed lower levels of pS6 but expressed increased levels of phosphorylated AMPK,

which inhibits pS6. Promoting S6 phosphorylation increased the proliferation rate of BAP1-deficient cells. *BAP1* mutant patient UM tumors and PDX models also expressed low levels of pS6, and *BAP1* mutant PDXs grew more slowly in vivo. The slow proliferation of BAP1-deficient UM cells and low pS6 expression are associated with better cell survival under amino acid starvation.

BAP1 alterations are also detected in malignant mesothelioma, renal cell carcinoma, cholangiocarcinoma, and (at lower frequencies) in cutaneous melanoma and breast cancer (22). Early studies suggested that BAP1 acts as a tumor suppressor as re-expression of *BAP1* WT in a BAP1-null human non-small lung cancer cell line inhibited cell cycle progression (23). Heterozygous knock-out of *BAP1* increased the development of malignant mesothelioma in mice injected peritoneally with crocidolite asbestos (24). Similar findings were expected for UM, given that the loss of BAP1 has been associated with larger tumors and an elevated risk of metastasis in patients (25). However, knockdown of *BAP1* decreased UM cell proliferation and induced cell cycle arrest (11). Consistent with this, we observed more rapid proliferation of UM cells following BAP1 re-expression in *BAP1*-deficient cells. The increase in cell proliferation was actually lower than the proliferation rate of parental *BAP1* WT cells. This could be due to cell line-specific differences or that other components apart from BAP1 may also regulate cell proliferation. Similar to our findings, *BAP1* knockdown in breast cancer models diminished cell proliferation (26, 27). Thus, the role of BAP1 appears to be context dependent and complex. It will be important in future studies to identify effects of BAP1 loss in non-BAP1 related tissues and whether there are commonalities.

BAP1 expression correlated with pS6 and pp70S6K1 levels. S6 is a ribosomal protein of the 40S subunit of eukaryotic ribosomes and is phosphorylated downstream of the mechanistic target of rapamycin complex 1 (mTORC1) or MAPK signaling pathways. The mTOR–p70S6K1–S6 pathway responds to growth factors and nutrients and promotes protein translation and cell proliferation (19, 30). The abundance of pS6 was markedly higher in BAP1-proficient cells, although some BAP1-WT cell lines had low levels of pS6, including UM002B and UM004. In the PDX models, whereas both BAP1 mutant models had lower pS6 levels and grew more slowly than BAP1-WT PDX1901 in vivo, the BAP1-mutant PDX1904 had higher pS6 compared to the *BAP1* mutant PDX1905. This suggests that factors beyond BAP1 status are likely involved in regulating pS6 in patient tumors. In future studies, it will be important to characterize this pS6 heterogeneity and, if additional resources are available, to include more PDXs and to detect pS6 at various time-points. Nevertheless, our findings indicate that intra-tumoral heterogeneity of pS6 exists but overall BAP1 loss is associated with low pS6 levels and BAP1 deficiency decreases pS6.

BAP1 loss is associated with aggressiveness of UM and elevated risk of metastasis. We postulate that the slow proliferation phenotype and low pS6 of BAP1-deficient UM cells are characteristics of tumor cells undergoing metastatic dissemination rather than late-stage aggressive macro-metastases that are rapidly proliferating and are linked to cellular processes required for metastasis. Low pS6 levels tend to correlate with improved patient survival in various cancer types (38, 39), better response to targeted therapies such as MEK inhibitors (40, 41), and decreased cell migration (42, 43). However, cell proliferation and

protein translation through pS6 are energy- and nutrient-consuming processes; hence, low pS6 potentially promotes UM cell survival in stressed conditions and microenvironments. We found here that BAP1-deficient UM cells survived better under amino acid starvation and this was reversed by expression of active S6K1 which increased pS6 and cell proliferation. Future studies will aim to identify the precise mechanism sustaining the survival of cells, and its role in metastasis. Unfortunately, a suitable in vivo metastasis model of UM from the primary tumor is currently lacking. An intrasplenic injection model of UM leading to cell colonization of the liver has been established (44), but it bypasses the initial steps of metastasis, including survival in the bloodstream, which is a likely important part of the mechanism of survival under amino acid starvation (45).

BAP1-deficient UM with low pS6 and slow proliferation may also undergo other processes associated with metastasis. For example, autophagy has been linked to an increased risk of cancer metastasis and low pS6 (46–48). BAP1-deficient cells may be undergoing dormancy/quiescence and a slow-cycling phenotype that has been linked to metastasis and drug resistance (49–51). We hypothesize that under certain conditions that can alter the liver microenvironment—such as liver fibrosis, aging, and fatty liver—increase the secretion of growth factors and cytokines that may activate S6 in the UM cells and result in rapidly proliferating macro-metastases.

In conclusion, our findings show effects of BAP1 deficiency on the proliferation of UM cells and low levels of phosphorylated S6. Our findings were consistent in UM patient samples and growth of *BAP1* mutant PDX models. We found that the slow proliferation of BAP1-deficient UM cells and low pS6 were associated with better cell survival during amino acid starvation, which may contribute to metastasis. Overall, our findings suggest that BAP1 mediates growth effects in UM and that further characterization of BAP1-mediated pathways and processes may inform the development of strategies to improve treatment efficacy in UM patients.

Materials and Methods

Cell culture:

Uveal melanoma cell lines MP46, MP65, MP38, MM66, and MM28 were obtained from S. Roman-Roman (Institute of Curie, France) and maintained in RPMI supplemented with 20% FBS (54). 92.1 was obtained from M. Jager (Leiden University, The Netherlands) and grown in RPMI containing 10% heat-inactivated FBS and 2 mmol/L L-glutamine. UM001, UM004, UM002B, and PDX4 cells were established at Thomas Jefferson University and grown as reported previously (55). UM002B and PDX4 were cultured in the same conditions as UM001 and UM004, respectively. OMM1.3 was provided by B. Ksander's laboratory (Harvard Medical School, USA) and cultured in RPMI and 10% FBS. WM3618F was purchased from Rockland Immunochemicals (Pottstown, Pennsylvania, USA) and grown according to manufacturer's instructions. HEK293 cells were cultured in DMEM and 10% FBS. Amino acid-free culture media was purchased from Caisson Labs (Smithfield, Utah, USA). All cell culture media were supplemented with 50 IU penicillin and 50 μg/ml streptomycin. Cell lines were regularly monitored for mycoplasma contamination and by short tandem repeat (STR) analysis for authentication.

Patient specimens and PDX models:

Tissue procurement was approved by the Institutional Review Board of Thomas Jefferson University (approval number 02.9014R). Patient liver metastatic tumor specimens, UMT205B, UMT-18–8-2, and UMT-21–12A, were fixed in buffered formalin and embedded in paraffin. The PDXs were generated from patient metastatic tumor lesions by growing the specimens for 2 to 3 passages in NOD SCID gamma (NSG) mice. The mutational status of each PDX is shown in table S2.

Lentiviral transduction:

Plasmids were purchased from Addgene (Watertown, Massachusetts, USA). Plasmids used were *BAP1* WT (pLVX-M-Flag-BAP1, #125840), *BAP1* C91A (pLVX-M-Flag-BAP1-C91A, #125841), *BAP1* C91G (pLVX-M-Flag-BAP1-C91G, #125845), empty vector (pLVX-M-puro, #125839), pRK7-HA-S6K1-E389-ΔCT (#8993) and pDONR223-RPS6KB1 (#23686). All plasmid DNA were purified using a DNA Maxiprep purification kit (Thermo Fisher Scientific; Waltham, Massachusetts, USA). S6K1-E389-ΔCT and S6K1 WT were cloned from pRK7-HA-S6K1-E389-ΔCT or pDONR223-RPS6KB1, respectively, into pENTR and pLENTI-puro vectors by PCR. Lentivirus was then generated using HEK293 cells. UM cells were infected with lentivirus and selected according to the antibiotic resistance genes of each plasmid.

siRNA transfection:

siRNAs were purchased from Dharmacon (Horizon Discovery) (Lafayette, Colorado, USA). si-*BAP1* #1 (GAGUUCAUCUGCACCUUUA), si-*BAP1* #2 (CCACAAGUCUCAAGAGUCA) and si-Control (On-Target control; UGGUUUACAUGUCGACUAAUU) were used. Cells were seeded at 40 to 50% confluency and transfected with the siRNA (25 nM final concentration) using the Lipofectamine RNAiMax transfection reagent (Invitrogen; Waltham, Massachusetts, USA).

Cell viability:

Cells were seeded in 6-well plates at 2.5×10^5 cells per well for long-term (5 to 7 days) experiments and 4×10^5 cells per well for short-term (3 days) experiments. For the crystal violet experiments, cells were rinsed in PBS and incubated with 0.2% (w/v) crystal violet in buffered (1:10 dilution) formalin for 1 to 2 hours on a shaker. Cells were then washed twice with de-ionized water before culture plates were air-dried overnight. High magnification (40x) images of cells were captured using the Nikon Eclipse Ti-E microscope (Nikon, Japan). Quantitation of crystal violet staining of viable cells was performed using ImageJ on the 40x magnification images (56). For the Incucyte® experiments, cells grown on culture plates were inserted into the Incucyte® live cell imager and cell confluency was measured and analyzed using the accompanying software.

Western blotting:

Analysis of protein expression has been described previously (16, 57). Briefly, cells were lysed in Laemmli sample buffer (Bio-Rad; Hercules, California, USA) containing β-mercaptoethanol. Proteins were separated by SDS-PAGE and transferred onto PVDF

membranes. Membranes were blocked for 60 to 90 min in 3% BSA in TBST and incubated with primary antibody diluted in 1% BSA in TBST overnight at 4°C. The membranes were then washed 3 × 10 min in TBST and incubated with a secondary antibody diluted in 1% skim milk in TBST for 90 min at room temperature. The membranes were washed 3 × 10 min in TBST and protein expression probed by chemiluminescence. Primary antibodies from Cell Signaling Technology (Danvers, Massachusetts, USA) were BAP1 (#13271), HSP90 (#4877), pS6 ($Ser^{235/236}$) (#4857), pS6 ($Ser^{240/244}$) (#2215), S6 (#2217), p-p70S6K1 (Thr^{389}) (#9234), p70S6K1 (#2708), pmTOR (Ser^{2448}) (#2971), mTOR (#2972), Aurora A (#14475), pAKT (Ser^{473}) (#4060), AKT (#4691), pAMPKα (Thr^{172}) (#2535), and AMPKα (#2603). All antibodies were diluted 1:1,000 in 1% BSA in TBST. The β-actin antibody (#A2066) was purchased from Sigma-Aldrich (St. Louis, Missouri, USA) and diluted 1:3,000 in 1% BSA in TBST.

3D Matrigel:

8-well chambers were pre-coated with Matrigel, then 500 cells were mixed with Matrigel (final concentration of 3% v/v) and added to each well. Medium containing 5% FBS was added to the layers in each well. Culture medium was changed after two days and, at day 4, numbers of single and multi-cell cluster events were calculated. To stain for pS6, cells were fixed with 4% paraformaldehyde for 20 min. Cells were then rinsed with 1x PBS-Glycine for 10 minutes and permeabilized with 1% Triton-X in PBS for 5 min. After rinsing the cells, blocking buffer (3% BSA and 1.5% normal goat serum in PBS) was added to the wells. After 60 min of blocking, the cells were incubated overnight at 4°C with the pS6 primary antibody (Cell Signaling #4857) at 1:200 diluted in blocking buffer. The cells were then washed once in PBS containing 0.02% Tween-20 for 30 min and then incubated with blocking buffer for 60 min. Then, secondary antibody diluted at 1:200 in blocking buffer was added to the cells and after 60 min of incubation at room temperature, the cells were washed for 30 min and incubated with Hoechst 33342 (nuclei stain) at 1:2,000 for 15 min. The cells were then washed for 30 min, mounted with Prolong anti-fade and allowed to air-dry overnight at room temperature. The slides were analyzed for pS6 staining using the Leica SP5 confocal microscope (Leica Microsystems, Germany).

Reverse Phase Protein Array (RPPA):

RPPA was performed at the MD Anderson Cancer Center RPPA facility. Cells were lysed and prepared according to the facility's lysis protocol for cells in 6-well plates. Briefly, cells were washed twice in PBS and then lysed in buffer containing 1% Triton X-100, 50 mM HEPES, pH 7.4, 150 mM NaCl, 1.5 mM MgCl2, 1 mM EGTA, 100 mM NaF, 10 mM Na pyrophosphate, 1 mM Na3VO4, 10% glycerol, and protease and phosphatase inhibitors that were freshly added prior to lysis. Lysates were then collected and centrifuged for 10 min at 14,000 rpm at 4°C. The supernatant was retrieved, and protein concentration was determined using the Bradford protein assay (Bio-rad). Cell lysates were mixed with 4x SDS buffer (40% Glycerol, 8% SDS, 0.25 M Tris-HCL, pH 6.8) containing β-mercaptoethanol (1:10 v/v) and boiled for 5 min. Antibodies against 492 proteins were tested in the RPPA. Analysis of RPPA data was performed as described previously (55). A list of genes associated with regulation of cell proliferation (table S1) was obtained from the Gene Set Enrichment Analysis (GSEA) website and expression of total and phosphorylated

levels of corresponding proteins were evaluated in the RPPA. Storey q-values calculations in heatmaps comparing BAP1-deficient to *BAP1* WT or BAP1 re-expressing UM were conducted in MATLAB (v2017b) using the mattest and mafdr functions.

Analysis of The Cancer Genome Atlas (TCGA) UM data:

TCGA data were retrieved from https://www.cancer.gov/tcga. All UM patient samples (n=80) were from primary UM tumors. RPPA data were available for only 12 samples and data were analyzed for differences in pS6 based on BAP1 status or expression.

Single cell RNA sequencing analysis:

Single cell RNA sequencing data from 11 UM patient tumor samples (8 primary and 3 metastatic) was obtained from the GEO database (Accession GSE139829) and processed using the Seurat package (v3.1.4) (58, 59). Cell types were identified using methods described previously (59) and data was normalized using the SCTransform method (60) with regression based on the percent mitochondrial content. The ggplot2 package (v3.3.2 https://ggplot2.tidyverse.org) was used to generate plots and data analyses were performed in R (v4.0.2 http://www.R-project.org/).

In vivo xenograft growth:

All animal experiments were approved by the Institutional Animal Care and Use Committee and performed at the Thomas Jefferson University animal facility that is accredited by the Association for the Assessment and Accreditation of Laboratory Animal Care. For subcutaneous injection experiments, NSG mice (8 weeks, females) were obtained from T. Manser (Thomas Jefferson University, USA). At least 5 animals were injected per group and mice not bearing tumors were removed as outliers. Each animal was injected subcutaneously with 5×10^6 UM cells in 100 μL PBS. Tumors were measured weekly using a digital caliper and tumor volume was calculated using this formula: volume = length × (width^2/2). Data from all animals except outliers will be included in quantitation and statistical analysis.
To grow PDX models intrahepatically in NSG mice, PDXs (PDX1901; passage three, PDX1904; passage three, and PDX1905; passage two) were implanted into the liver of NSG mice according to the protocol described previously (61). Computerized tomography (CT) scans of tumors were obtained every 1 to 3 weeks and, from these scans, the largest tumor diameters (mm) were measured. Data from all animals in this experiment were included in quantitation and statistical analysis. Depending on availability of PDXs, at least 3 mice or animals were injected or implanted.

Statistical analysis for PDX in vivo growth assay:

The repeated measures of largest diameters were analyzed using the longitudinal linear mixed effects (LME) model with random effects of animals. The fixed effects in the LME model included the PDX, week and their (week x PDX) interaction. A significant interaction term would indicate a significant difference in the growth rate across the PDX models, and a post-hoc analysis using the Hochberg method is conducted if significance is reached (62). The residuals were evaluated to validate the assumptions of the models.

Immunohistochemistry:

Paraffin-embedded tissue was sliced and fixed onto slides and stained by the Sidney Kimmel Cancer Center (SKCC) pathology shared resource facility. Slides were stained with primary antibodies against pS6 ($Ser^{235/236}$, Cell Signaling Technology #4857) at a 1:200 dilution, BAP1 (Santa Cruz Biotechnology sc-28383) at a 1:25 dilution or Ki-67 (Abcam #ab16667) at 1:75. ABC-alkaline phosphatase (AP) kits and methyl green counter stains were used. Slides were scanned using the Aperio Scanscope CS2 at 20x magnification. Images were analyzed using the Aperio ImageScope software where random fields of the specimen were captured. These images were then analyzed for staining intensity and abundance using ImageJ and a protocol described previously (56, 63). Briefly, color deconvolution was performed in ImageJ using the H-DAB option, background of staining removed by adjusting the maximum threshold value, and the mean gray value, which represents staining intensity, was collected.

Statistical analysis:

All experiments were performed at least three times and quantitative data are shown as the mean ± S.E.M. of data from at least triplicate experiments (biological repeats) unless stated otherwise. Data outliers were removed unless stated otherwise. Statistical significance was measured using unpaired student's t-test and p-values adjusted using the Hochberg method.

Supplementary Material

Refer to Web version on PubMed Central for supplementary material.

Acknowledgements:

We thank D. E. Fisher, Director of the Department of Defense, Melanoma Academy, for guidance and advice. We thank T. Manser at Thomas Jefferson University for providing the NSG mice. We also thank all personnel at the SKCC core facilities for their assistance with experiments. We thank S. Caksa, C. Capparelli, S. Varney, and D. Erkes (Thomas Jefferson University) for their valuable feedback during the preparation of this manuscript. We also thank J. Lo (Edith Cowan University) for reviewing the statistical methods used in this manuscript.

Funding:

V.C. is a recipient of the Department of Defense (DoD) Melanoma Academy Scholar Award. This work is also supported by a DoD Team Science award and a National Institutes of Health (NIH) National Cancer Institute (NCI) R01 CA253977 to A.E.A, and J.A.A-G. This work is also supported by the Samuel Waxman Cancer Research Foundation Tumor Dormancy Program, to J.A.A-G., who is also a Samuel Waxman Cancer Research Foundation Investigator. The RPPA Core (M.A.D.) is supported by NCI grant CA16672 and NIH grant R50 CA221675: Functional Proteomics by Reverse Phase Protein Array in Cancer.

Data and materials availability:

All data needed to evaluate the conclusions in the paper are present in the main paper or the Supplementary Materials.

References and Notes

1. Kaliki S, Shields CL. Uveal melanoma: relatively rare but deadly cancer. Eye (Lond). 2017;31(2):241–57. [PubMed: 27911450]

2. Diener-West M, Reynolds SM, Agugliaro DJ, Caldwell R, Cumming K, Earle JD, et al. Development of metastatic disease after enrollment in the COMS trials for treatment of choroidal melanoma: Collaborative Ocular Melanoma Study Group Report No. 26. Arch Ophthalmol. 2005;123(12):1639–43. [PubMed: 16344433]

3. Chua V, Mattei J, Han A, Johnston L, LiPira K, Selig SM, et al. The Latest on Uveal Melanoma Research and Clinical Trials: Updates from the Cure Ocular Melanoma (CURE OM) Science Meeting (2019). Clin Cancer Res. 2021;27(1):28–33. [PubMed: 33060121]

4. Orloff M Clinical Trials in Metastatic Uveal Melanoma: Immunotherapy. Ocul Oncol Pathol. 2021;7(3):168–76. [PubMed: 34307327]

5. Krantz BA, Dave N, Komatsubara KM, Marr BP, Carvajal RD. Uveal melanoma: epidemiology, etiology, and treatment of primary disease. Clin Ophthalmol. 2017;11:279–89. [PubMed: 28203054]

6. Chua V, Lapadula D, Randolph C, Benovic JL, Wedegaertner PB, Aplin AE. Dysregulated GPCR Signaling and Therapeutic Options in Uveal Melanoma. Mol Cancer Res. 2017;15(5):501–6. [PubMed: 28223438]

7. Decatur CL, Ong E, Garg N, Anbunathan H, Bowcock AM, Field MG, Harbour JW. Driver Mutations in Uveal Melanoma: Associations With Gene Expression Profile and Patient Outcomes. JAMA Ophthalmol. 2016;134(7):728–33. [PubMed: 27123562]

8. Martin M, Masshofer L, Temming P, Rahmann S, Metz C, Bornfeld N, et al. Exome sequencing identifies recurrent somatic mutations in EIF1AX and SF3B1 in uveal melanoma with disomy 3. Nat Genet. 2013;45(8):933–6. [PubMed: 23793026]

9. Szczepanski AP, Wang L. Emerging multifaceted roles of BAP1 complexes in biological processes. Cell Death Discov. 2021;7(1):20. [PubMed: 33483476]

10. Harbour JW, Onken MD, Roberson ED, Duan S, Cao L, Worley LA, et al. Frequent mutation of BAP1 in metastasizing uveal melanomas. Science. 2010;330(6009):1410–3. [PubMed: 21051595]

11. Matatall KA, Agapova OA, Onken MD, Worley LA, Bowcock AM, Harbour JW. BAP1 deficiency causes loss of melanocytic cell identity in uveal melanoma. BMC Cancer. 2013;13:371. [PubMed: 23915344]

12. Liu-Smith F, Lu Y. Opposite Roles of BAP1 in Overall Survival of Uveal Melanoma and Cutaneous Melanoma. J Clin Med. 2020;9(2).

13. Zhang W, Xia D, Li Z, Zhou T, Chen T, Wu Z, et al. Aurora-A/ERK1/2/mTOR axis promotes tumor progression in triple-negative breast cancer and dual-targeting Aurora-A/mTOR shows synthetic lethality. Cell Death Dis. 2019;10(8):606.

14. Porta C, Paglino C, Mosca A. Targeting PI3K/Akt/mTOR Signaling in Cancer. Front Oncol. 2014;4:64. [PubMed: 24782981]

15. Chomanicova N, Gazova A, Adamickova A, Valaskova S, Kyselovic J. The role of AMPK/mTOR signaling pathway in anticancer activity of metformin. Physiol Res. 2021;70(4):501–8. [PubMed: 34062070]

16. Chua V, Han A, Bechtel N, Purwin TJ, Hunter E, Liao C, et al. The AMP-dependent kinase pathway is upregulated in BAP1 mutant uveal melanoma. Pigment Cell Melanoma Res. 2021.

17. Gwinn DM, Shackelford DB, Egan DF, Mihaylova MM, Mery A, Vasquez DS, et al. AMPK phosphorylation of raptor mediates a metabolic checkpoint. Mol Cell. 2008;30(2):214–26. [PubMed: 18439900]

18. Inoki K, Zhu T, Guan KL. TSC2 mediates cellular energy response to control cell growth and survival. Cell. 2003;115(5):577–90. [PubMed: 14651849]

19. Thomas G, Martin-Perez J, Siegmann M, Otto AM. The effect of serum, EGF, PGF2 alpha and insulin on S6 phosphorylation and the initiation of protein and DNA synthesis. Cell. 1982;30(1):235–42. [PubMed: 6751557]

20. Aran D, Sirota M, Butte AJ. Systematic pan-cancer analysis of tumour purity. Nat Commun. 2015;6:8971. [PubMed: 26634437]

21. Chauvin C, Koka V, Nouschi A, Mieulet V, Hoareau-Aveilla C, Dreazen A, et al. Ribosomal protein S6 kinase activity controls the ribosome biogenesis transcriptional program. Oncogene. 2014;33(4):474–83. [PubMed: 23318442]

22. Carbone M, Yang H, Pass HI, Krausz T, Testa JR, Gaudino G. BAP1 and cancer. Nat Rev Cancer. 2013;13(3):153–9. [PubMed: 23550303]

23. Ventii KH, Devi NS, Friedrich KL, Chernova TA, Tighiouart M, Van Meir EG, Wilkinson KD. BRCA1-associated protein-1 is a tumor suppressor that requires deubiquitinating activity and nuclear localization. Cancer Res. 2008;68(17):6953–62. [PubMed: 18757409]
24. Xu J, Kadariya Y, Cheung M, Pei J, Talarchek J, Sementino E, et al. Germline mutation of Bap1 accelerates development of asbestos-induced malignant mesothelioma. Cancer Res. 2014;74(16):4388–97. [PubMed: 24928783]
25. Ewens KG, Lalonde E, Richards-Yutz J, Shields CL, Ganguly A. Comparison of Germline versus Somatic BAP1 Mutations for Risk of Metastasis in Uveal Melanoma. BMC Cancer. 2018;18(1):1172. [PubMed: 30477459]
26. Qin J, Zhou Z, Chen W, Wang C, Zhang H, Ge G, et al. BAP1 promotes breast cancer cell proliferation and metastasis by deubiquitinating KLF5. Nat Commun. 2015;6:8471. [PubMed: 26419610]
27. Machida YJ, Machida Y, Vashisht AA, Wohlschlegel JA, Dutta A. The deubiquitinating enzyme BAP1 regulates cell growth via interaction with HCF-1. J Biol Chem. 2009;284(49):34179–88. [PubMed: 19815555]
28. Lee HS, Lee SA, Hur SK, Seo JW, Kwon J. Stabilization and targeting of INO80 to replication forks by BAP1 during normal DNA synthesis. Nat Commun. 2014;5:5128. [PubMed: 25283999]
29. Yu H, Mashtalir N, Daou S, Hammond-Martel I, Ross J, Sui G, et al. The ubiquitin carboxyl hydrolase BAP1 forms a ternary complex with YY1 and HCF-1 and is a critical regulator of gene expression. Mol Cell Biol. 2010;30(21):5071–85. [PubMed: 20805357]
30. Holz MK, Ballif BA, Gygi SP, Blenis J. mTOR and S6K1 mediate assembly of the translation preinitiation complex through dynamic protein interchange and ordered phosphorylation events. Cell. 2005;123(4):569–80. [PubMed: 16286006]
31. Bononi A, Giorgi C, Patergnani S, Larson D, Verbruggen K, Tanji M, et al. BAP1 regulates IP3R3-mediated Ca(2+) flux to mitochondria suppressing cell transformation. Nature. 2017;546(7659):549–53. [PubMed: 28614305]
32. Biever A, Valjent E, Puighermanal E. Ribosomal Protein S6 Phosphorylation in the Nervous System: From Regulation to Function. Front Mol Neurosci. 2015;8:75. [PubMed: 26733799]
33. Roux PP, Shahbazian D, Vu H, Holz MK, Cohen MS, Taunton J, et al. RAS/ERK signaling promotes site-specific ribosomal protein S6 phosphorylation via RSK and stimulates cap-dependent translation. J Biol Chem. 2007;282(19):14056–64. [PubMed: 17360704]
34. House C, Wettenhall RE, Kemp BE. The influence of basic residues on the substrate specificity of protein kinase C. J Biol Chem. 1987;262(2):772–7. [PubMed: 3100520]
35. Yano T, Ferlito M, Aponte A, Kuno A, Miura T, Murphy E, Steenbergen C. Pivotal role of mTORC2 and involvement of ribosomal protein S6 in cardioprotective signaling. Circ Res. 2014;114(8):1268–80. [PubMed: 24557881]
36. Schumacher AM, Velentza AV, Watterson DM, Dresios J. Death-associated protein kinase phosphorylates mammalian ribosomal protein S6 and reduces protein synthesis. Biochemistry. 2006;45(45):13614–21. [PubMed: 17087515]
37. Hutchinson JA, Shanware NP, Chang H, Tibbetts RS. Regulation of ribosomal protein S6 phosphorylation by casein kinase 1 and protein phosphatase 1. J Biol Chem. 2011;286(10):8688–96. [PubMed: 21233202]
38. Cuperjani F, Gashi L, Kurshumliu F, Dreshaj S, Selimi F. Relationship between Ribosomal Protein S6-pS240 Expression and other Prognostic Factors in Non-Special Type Invasive Breast Cancer. Breast Care (Basel). 2019;14(3):171–5. [PubMed: 31316316]
39. Kim SH, Jang YH, Chau GC, Pyo S, Um SH. Prognostic significance and function of phosphorylated ribosomal protein S6 in esophageal squamous cell carcinoma. Mod Pathol. 2013;26(3):327–35. [PubMed: 22996377]
40. Corcoran RB, Rothenberg SM, Hata AN, Faber AC, Piris A, Nazarian RM, et al. TORC1 suppression predicts responsiveness to RAF and MEK inhibition in BRAF-mutant melanoma. Sci Transl Med. 2013;5(196):196ra98.
41. Hirashita Y, Tsukamoto Y, Yanagihara K, Fumoto S, Hijiya N, Nakada C, et al. Reduced phosphorylation of ribosomal protein S6 is associated with sensitivity to MEK inhibition in gastric cancer cells. Cancer Sci. 2016;107(12):1919–28. [PubMed: 27699948]

42. Olea-Flores M, Juarez-Cruz JC, Zuniga-Eulogio MD, Acosta E, Garcia-Rodriguez E, Zacapala-Gomez AE, et al. New Actors Driving the Epithelial-Mesenchymal Transition in Cancer: The Role of Leptin. Biomolecules. 2020;10(12).
43. Chen B, Tan Z, Gao J, Wu W, Liu L, Jin W, et al. Hyperphosphorylation of ribosomal protein S6 predicts unfavorable clinical survival in non-small cell lung cancer. J Exp Clin Cancer Res. 2015;34:126.
44. Sugase T, Lam BQ, Danielson M, Terai M, Aplin AE, Gutkind JS, Sato T. Development and optimization of orthotopic liver metastasis xenograft mouse models in uveal melanoma. J Transl Med. 2020;18(1):208. [PubMed: 32434572]
45. O'Brien M, Ernst M, Poh AR. An intrasplenic injection model of pancreatic cancer metastasis to the liver in mice. STAR Protoc. 2023;4(1):102021. [PubMed: 36638017]
46. Kang HT, Lee KB, Kim SY, Choi HR, Park SC. Autophagy impairment induces premature senescence in primary human fibroblasts. PLoS One. 2011;6(8):e23367. [PubMed: 21858089]
47. Sun J, Mu Y, Jiang Y, Song R, Yi J, Zhou J, et al. Inhibition of p70 S6 kinase activity by A77 1726 induces autophagy and enhances the degradation of superoxide dismutase 1 (SOD1) protein aggregates. Cell Death Dis. 2018;9(3):407. [PubMed: 29540819]
48. Zoncu R, Efeyan A, Sabatini DM. mTOR: from growth signal integration to cancer, diabetes and ageing. Nat Rev Mol Cell Biol. 2011;12(1):21–35. [PubMed: 21157483]
49. Basu S, Dong Y, Kumar R, Jeter C, Tang DG. Slow-cycling (dormant) cancer cells in therapy resistance, cancer relapse and metastasis. Semin Cancer Biol. 2022;78:90–103. [PubMed: 33979674]
50. Neophytou CM, Kyriakou TC, Papageorgis P. Mechanisms of Metastatic Tumor Dormancy and Implications for Cancer Therapy. Int J Mol Sci. 2019;20(24).
51. Capparelli C, Purwin TJ, Glasheen M, Caksa S, Tiago M, Wilski N, et al. Targeting SOX10-deficient cells to reduce the dormant-invasive phenotype state in melanoma. Nat Commun. 2022;13(1):1381. [PubMed: 35296667]
52. Sosa MS, Avivar-Valderas A, Bragado P, Wen HC, Aguirre-Ghiso JA. ERK1/2 and p38alpha/beta signaling in tumor cell quiescence: opportunities to control dormant residual disease. Clin Cancer Res. 2011;17(18):5850–7. [PubMed: 21673068]
53. Sosa MS, Parikh F, Maia AG, Estrada Y, Bosch A, Bragado P, et al. NR2F1 controls tumour cell dormancy via SOX9- and RARbeta-driven quiescence programmes. Nat Commun. 2015;6:6170. [PubMed: 25636082]
54. Amirouchene-Angelozzi N, Nemati F, Gentien D, Nicolas A, Dumont A, Carita G, et al. Establishment of novel cell lines recapitulating the genetic landscape of uveal melanoma and preclinical validation of mTOR as a therapeutic target. Mol Oncol. 2014;8(8):1508–20. [PubMed: 24994677]
55. Cheng H, Chua V, Liao C, Purwin TJ, Terai M, Kageyama K, et al. Co-targeting HGF/cMET Signaling with MEK Inhibitors in Metastatic Uveal Melanoma. Mol Cancer Ther. 2017;16(3):516–28. [PubMed: 28138035]
56. Schneider CA, Rasband WS, Eliceiri KW. NIH Image to ImageJ: 25 years of image analysis. Nat Methods. 2012;9(7):671–5. [PubMed: 22930834]
57. Chua V, Orloff M, Teh JL, Sugase T, Liao C, Purwin TJ, et al. Stromal fibroblast growth factor 2 reduces the efficacy of bromodomain inhibitors in uveal melanoma. EMBO Mol Med. 2019;11(2).
58. Butler A, Hoffman P, Smibert P, Papalexi E, Satija R. Integrating single-cell transcriptomic data across different conditions, technologies, and species. Nature biotechnology. 2018;36(5):411–20.
59. Durante MA, Rodriguez DA, Kurtenbach S, Kuznetsov JN, Sanchez MI, Decatur CL, et al. Single-cell analysis reveals new evolutionary complexity in uveal melanoma. Nat Commun. 2020;11(1):496. [PubMed: 31980621]
60. Stuart T, Butler A, Hoffman P, Hafemeister C, Papalexi E, Mauck III WM, et al. Comprehensive integration of single-cell data. Cell. 2019;177(7):1888–902. e21. [PubMed: 31178118]
61. Ozaki S, Vuyyuru R, Kageyama K, Terai M, Ohara M, Cheng H, et al. Establishment and Characterization of Orthotopic Mouse Models for Human Uveal Melanoma Hepatic Colonization. Am J Pathol. 2016;186(1):43–56. [PubMed: 26613897]

62. Hochberg Y A sharper Bonferroni procedure for multiple tests of significance. Biometrika. 1988;75(4):800–2.

63. Crowe AR, Yue W. Semi-quantitative Determination of Protein Expression using Immunohistochemistry Staining and Analysis: An Integrated Protocol. Bio Protoc. 2019;9(24).

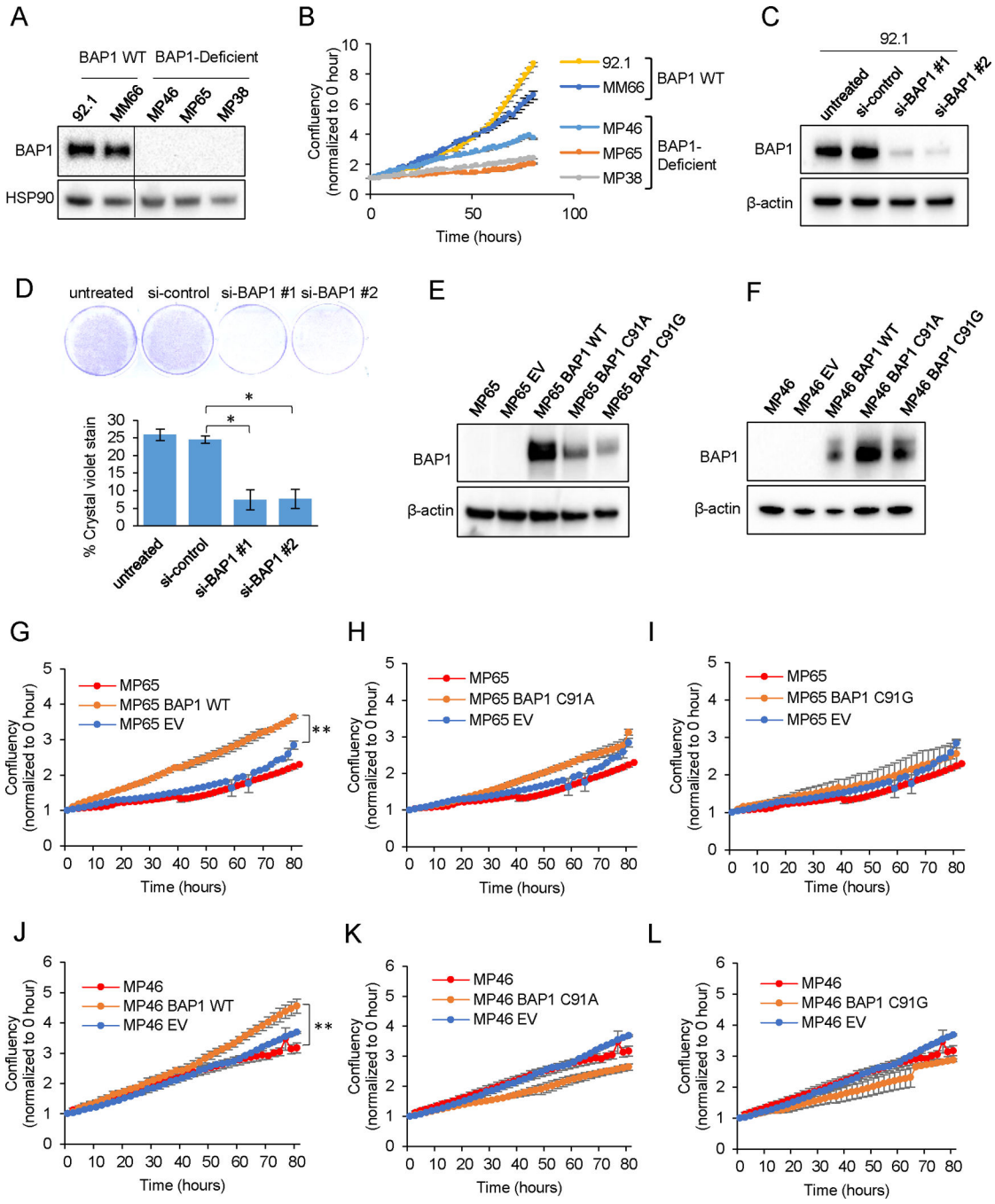

Figure 1: Loss of BAP1 is associated with slow proliferation of UM cells in 2D cultures.

(A) BAP1 protein expression in *BAP1* WT (92.1, MM66) and BAP1-deficient (MP46, MP65, MP38) UM cell lines detected by Western blotting. **(B)** Cell confluency measured over time using the Incucyte® live cell imager. Fold change in cell confluency normalized to confluency at 0 hour is shown. Mean data from triplicate experiments (N=3) is shown. **(C)** BAP1 protein levels in 92.1 cells following 72 hours of transfection with *BAP1* siRNA. **(D)** Crystal violet staining of 92.1 cells after si-*BAP1* transfection for 72 hours. Representative crystal violet images and mean ± S.E.M. of % crystal violet staining from

triplicate experiments (N=3) are shown. *p≤0.05 by unpaired student's t-test adjusted using the Hochberg method. **(E and F)** Western blot of BAP1 protein levels in MP65 and MP46 cells transduced with empty vector (EV), WT or DUB-mutant *BAP1* (C91A or C91G). **(G to L)** Cell confluency of MP65 or MP46 parental cells compared to cells transduced with EV (empty vector), *BAP1* WT, *BAP1* C91A, or *BAP1* C91G. Cell confluency was determined using the Incucyte® live cell imager and normalized to confluency at 0 hour. Mean ± S.E.M. of cell confluency from triplicate experiments (N=3) is shown. **p≤0.01 by unpaired student's t-test adjusted using the Hochberg method.

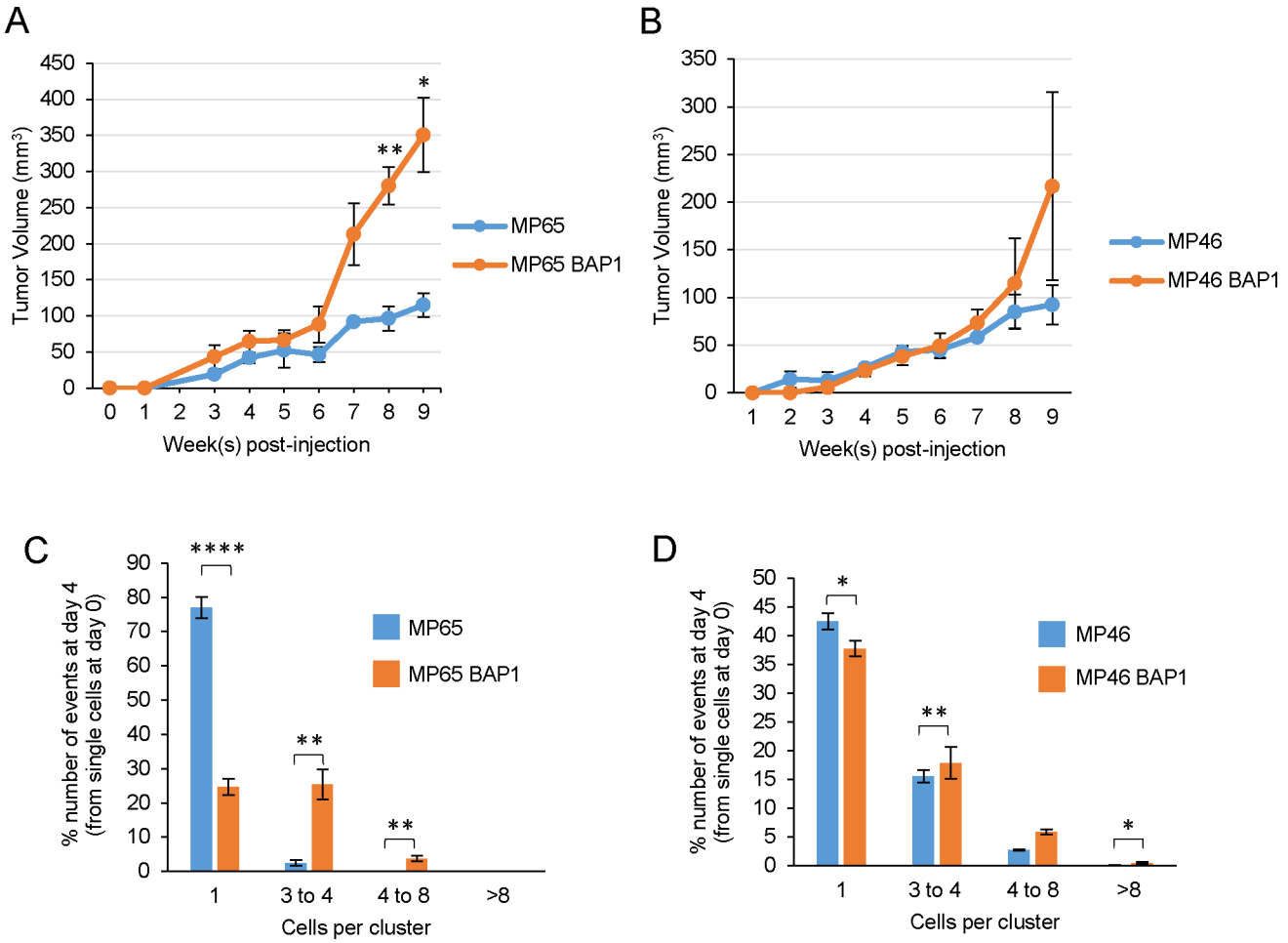

Figure 2: Re-expression of BAP1 increased the proliferation of UM cells in vivo and in 3D cultures.

(A) Tumor volume of MP65 and MP65 BAP1 WT, and **(B)** MP46 and MP46 BAP1 WT xenografts measured weekly following subcutaneous injection of cells in NSG mice. Mean ± S.E.M. of tumor volume from four animals (N=4) is shown. *p≤0.05, **p≤0.01 by unpaired student's t-test adjusted using the Hochberg method. **(C)** Percentage of single-cell or multi-cell cluster events measured at four days after seeding single MP65 or MP65 BAP1 WT and **(D)** MP46 or MP46 BAP1 WT cells in 3D Matrigel. Bar graphs show mean ± S.E.M. from triplicate experiments (N=3). *p≤0.05, **p≤0.01, ****p≤0.0001 by unpaired student's t-test adjusted using the Hochberg method.

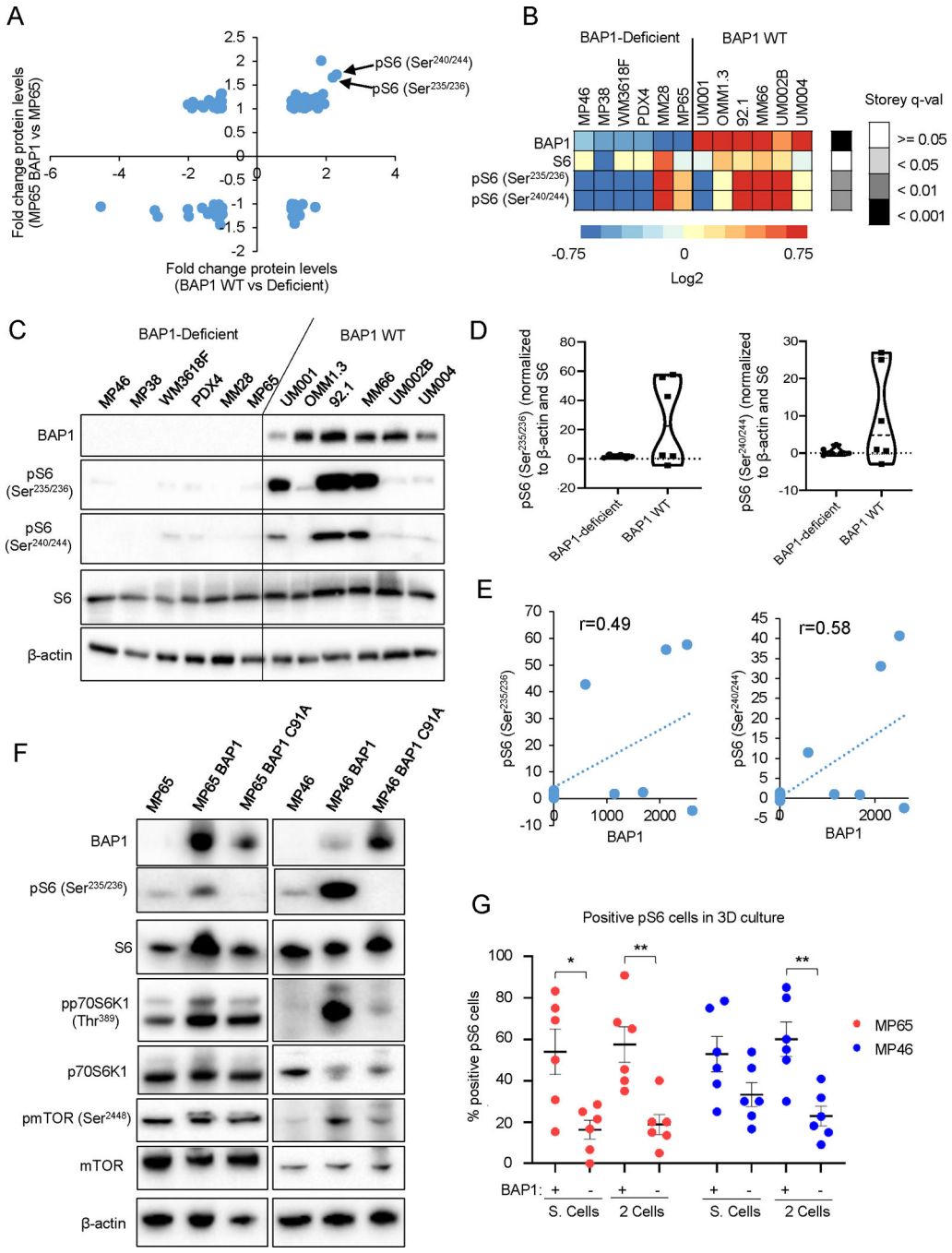

Figure 3: S6 phosphorylation is low in BAP1-deficient UM cells.

(A) Dot-plot showing proteins up- or down-regulated in MP65 BAP1 compared to MP65 parental cells and in a panel of *BAP1* WT compared to BAP1-deficient UM cells. Results were derived from analysis of RPPA data and focused on proteins associated with cell proliferation. **(B)** Heatmap showing median centered log2-transformed expression of pS6 and S6 protein levels from RPPA data in a panel of BAP1-deficient and *BAP1* WT UM cell lines. Statistical significance of the protein expression between BAP1-deficient and *BAP1* WT was determined using Storey q-values (N=4). **(C)** Validation of pS6 protein levels in

a UM cell line panel by Western blotting. **(D)** Violin plots of quantitation of pS6 from Western blots in (C) and determined by densitometry. pS6 levels shown were normalized to β-actin and S6. **(E)** Correlation coefficient of BAP1 and pS6 ($Ser^{235/236}$) or pS6 ($Ser^{240/244}$) levels from quantitation of blots in (C). **(F)** Western blot analysis of phosphorylated (p) S6, p70S6K1, and mTOR in MP65 or MP46 re-expressing *BAP1* WT or *BAP1* C91A. Representative blots from triplicate experiments or lysates (N=3) are shown. **(G)** Percentage of cells positive for pS6 ($Ser^{235/236}$) in MP65 or MP46 parental cells and cells transduced with *BAP1* WT. Data was collected from single and 2-cell clusters after 4 days of seeding in 3D Matrigel. Graphs show mean ± S.E.M. from triplicate experiments (N=3). *p≤0.05, **p≤0.01 by unpaired student's t-test adjusted using the Hochberg method.

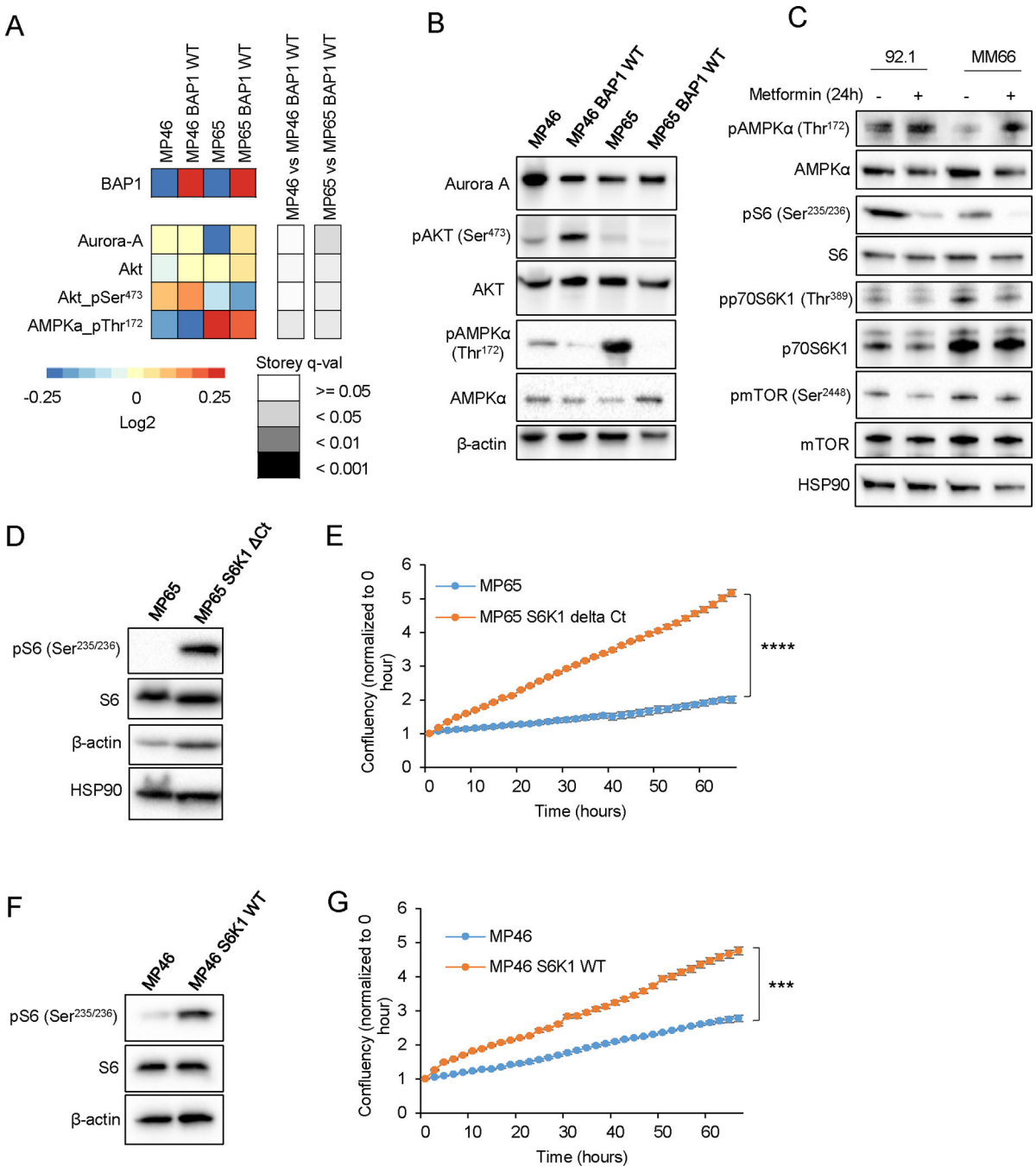

Figure 4: Mechanisms associated with low pS6 and slow proliferation of BAP1-deficient UM cells.

(A) Heatmap of expression of proteins associated with mTOR/S6 signaling in BAP1-deficient (MP46 and MP65) and BAP1 re-expressing (MP46 BAP1 WT and MP65 BAP1 WT) cells. Proteins that are differentially expressed between the BAP1-deficient and BAP1 re-expressing cells are shown. Statistical significance of the protein expression between BAP1-deficient and BAP1 re-expressing cells was determined using Storey q-values (N=4). **(B)** Western blot analysis of proteins associated with mTOR/S6 signaling. **(C)** *BAP1* WT

cells, 92.1 and MM66, were treated with 10mM metformin for 24 hours and then expression of mTOR signaling pathway proteins were evaluated by Western blotting. **(D)** Western blotting for pS6 levels in MP65 transduced with active S6K1 (S6K1 E389 ΔCT). **(E)** Cell confluency of MP65 and MP65 S6K1 delta Ct. Cell confluency was determined using the Incucyte® live cell imager and normalized to confluency at 0 hour. Mean ± S.E.M. of cell confluency from triplicate experiments (N=3) is shown. ****p≤0.0001 by unpaired student's t-test adjusted using the Hochberg method. **(F)** pS6 levels determined by Western blotting in MP46 cells transduced with S6K1 WT. **(G)** Cell confluency of MP46 and MP46 S6K1 WT. Cell confluency was determined using the Incucyte® live cell imager and normalized to confluency at 0 hour. Mean ± S.E.M. of cell confluency from triplicate experiments (N=3) is shown. ***p≤0.001 by unpaired student's t-test adjusted using the Hochberg method.

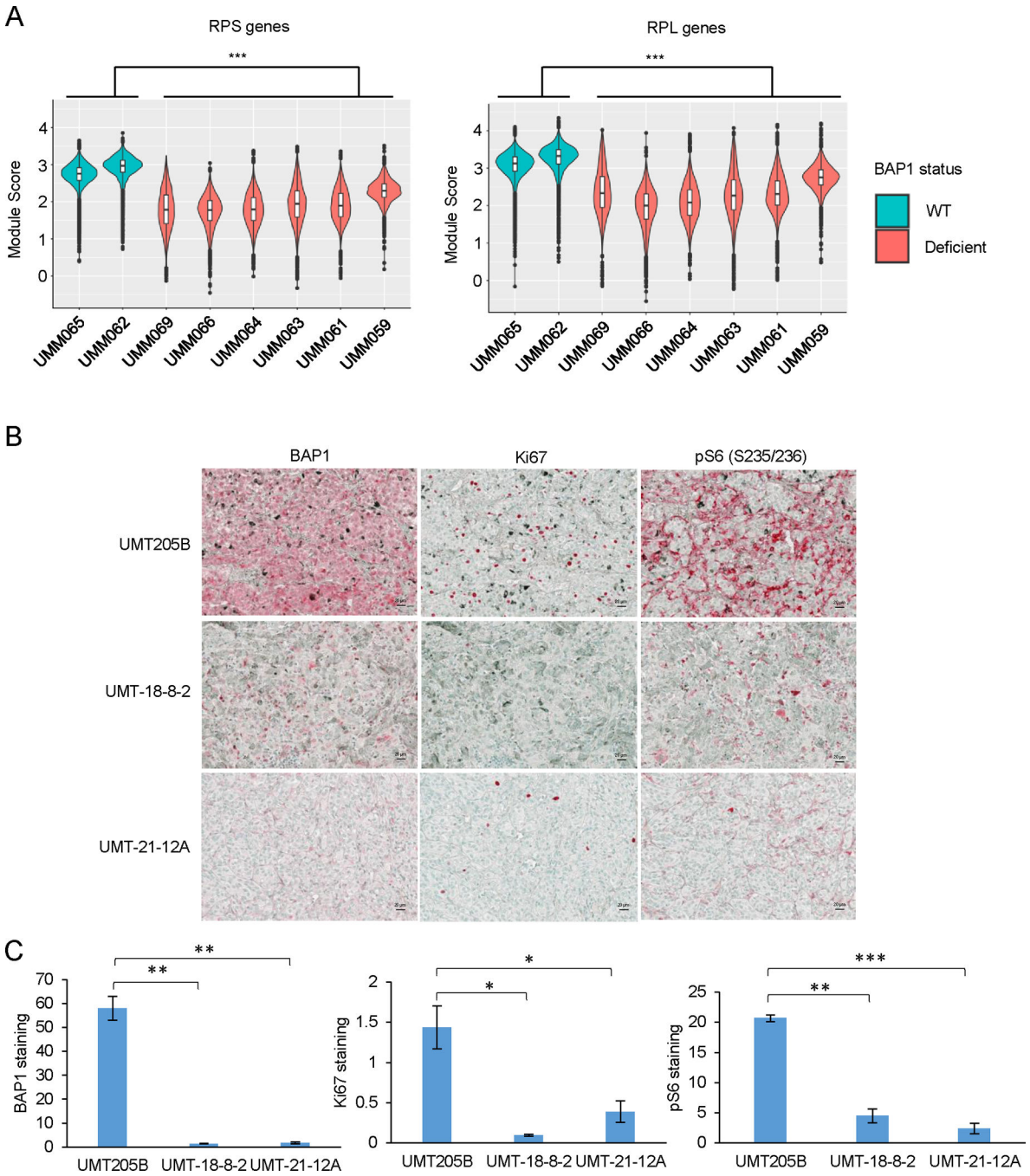

Figure 5: pS6 levels in UM patient tumors.

(A) Violin plots from single cell RNA sequencing data displaying average expression of ribosomal biogenesis genes regulated by S6K1 (*RPS* and *RPL* genes) in primary BAP1-deficient and BAP1 WT UM patient tumors (N = 6 and 2, respectively). Significance was assessed by the Mann-Whitney test, ***p< 0.001. Violin plots contain box and whisker plots, displaying the interquartile range, median, and minimum/maximum values. **(B)** Immunohistochemical staining of BAP1, Ki-67 and pS6 ($Ser^{235/236}$) in liver metastatic UM patient specimens. 400x magnification. Scale bar, 20 μm. **(C)** Quantitation of BAP1,

Ki-67, and pS6 staining in liver metastatic UM patient specimens. Three random fields at 400x magnification from 3 samples were captured and analyzed using ImageJ. *p≤0.05, **p≤0.01, ***p≤0.001 by unpaired student's t-test s adjusted using the Hochberg method.

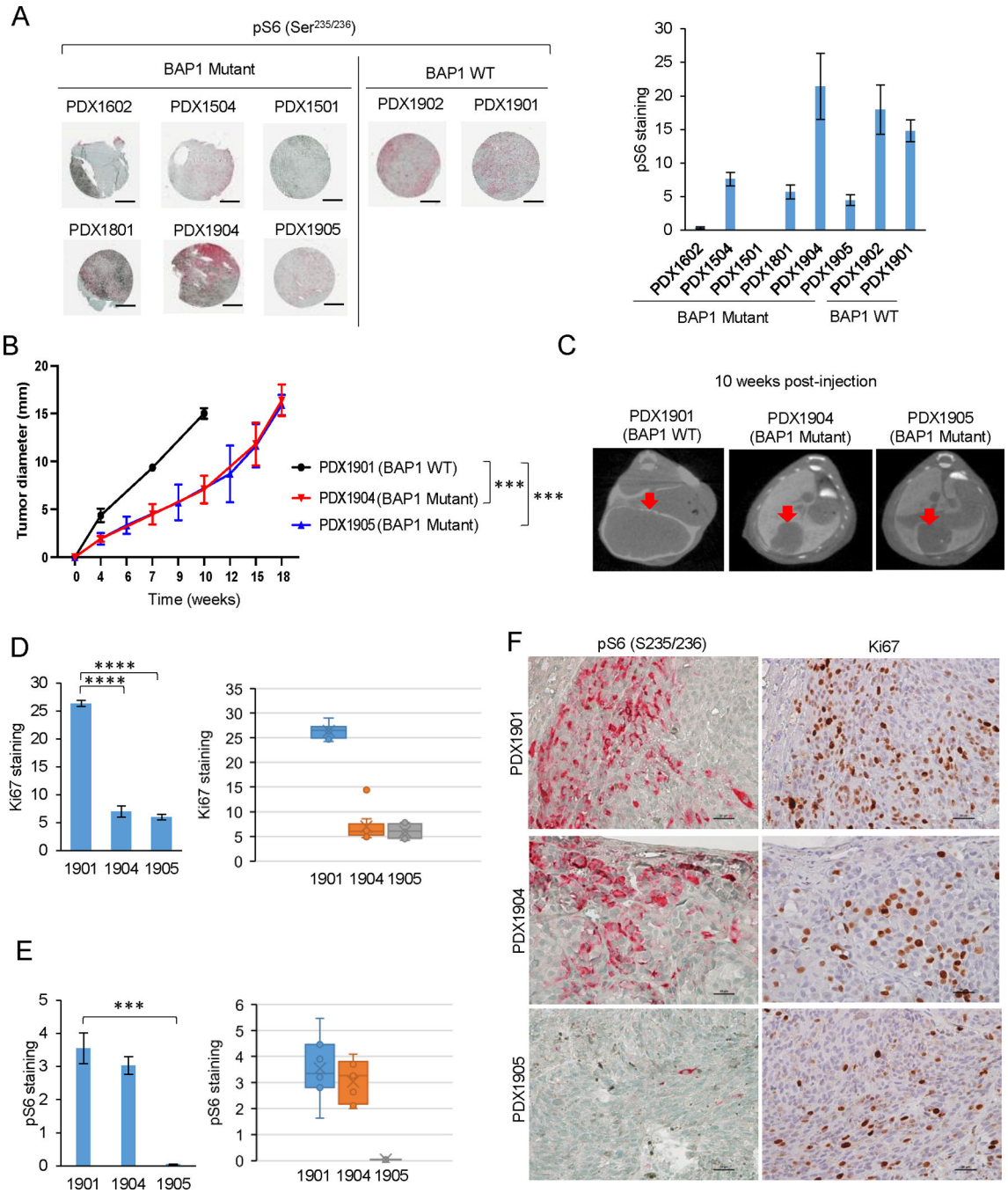

Figure 6: *BAP1* mutant PDX models of metastatic UM patient specimens express low pS6 levels and proliferate slower in vivo.

(A) pS6 staining by immunohistochemistry in PDXs originating from UM patient metastatic samples. PDXs in a tissue microarray were stained for pS6 (Ser$^{235/236}$), and staining was compared between *BAP1* mutant (N=6) and WT (N=2) PDXs, assigned on the basis of the available sequencing data of mutations of the specimens. Scale bar, 600 μm. Three random fields (400x magnification) of pS6 staining were captured for each PDX and the intensity and abundance of pS6 staining (red/pink) were measured using ImageJ,

right of the immunohistochemical staining. **(B)** Two *BAP1* mutant PDXs and one *BAP1* WT PDX were independently implanted intrahepatically into the liver of NSG mice, and tumor size was monitored by CT scanning. N=4 mice per PDX. ***p≤0.001 by the LME model with random effects of animals and a post-hoc analysis using the Hochberg method. **(C)** Representative transverse CT scans of the abdomen of mice 10 weeks after injection with the indicated PDX. **(D and E)** Quantitation of pS6 ($Ser^{235/236}$) and Ki-67 immunohistochemical staining of PDXs isolated at the last time point following sacrifice. Eight to ten random fields (400x magnification) of pS6 and Ki-67 staining were captured for each PDX tissue, and the intensity and abundance of staining were measured using ImageJ. Data are the mean ± S.E.M. of staining (N=8–10). ***p≤0.001, ****p≤0.0001 by unpaired student's t-test adjusted using the Hochberg method. **(F)** Representative images of immunohistochemical staining for pS6 and Ki-67 in the PDXs. Scale bar, 20 μm.

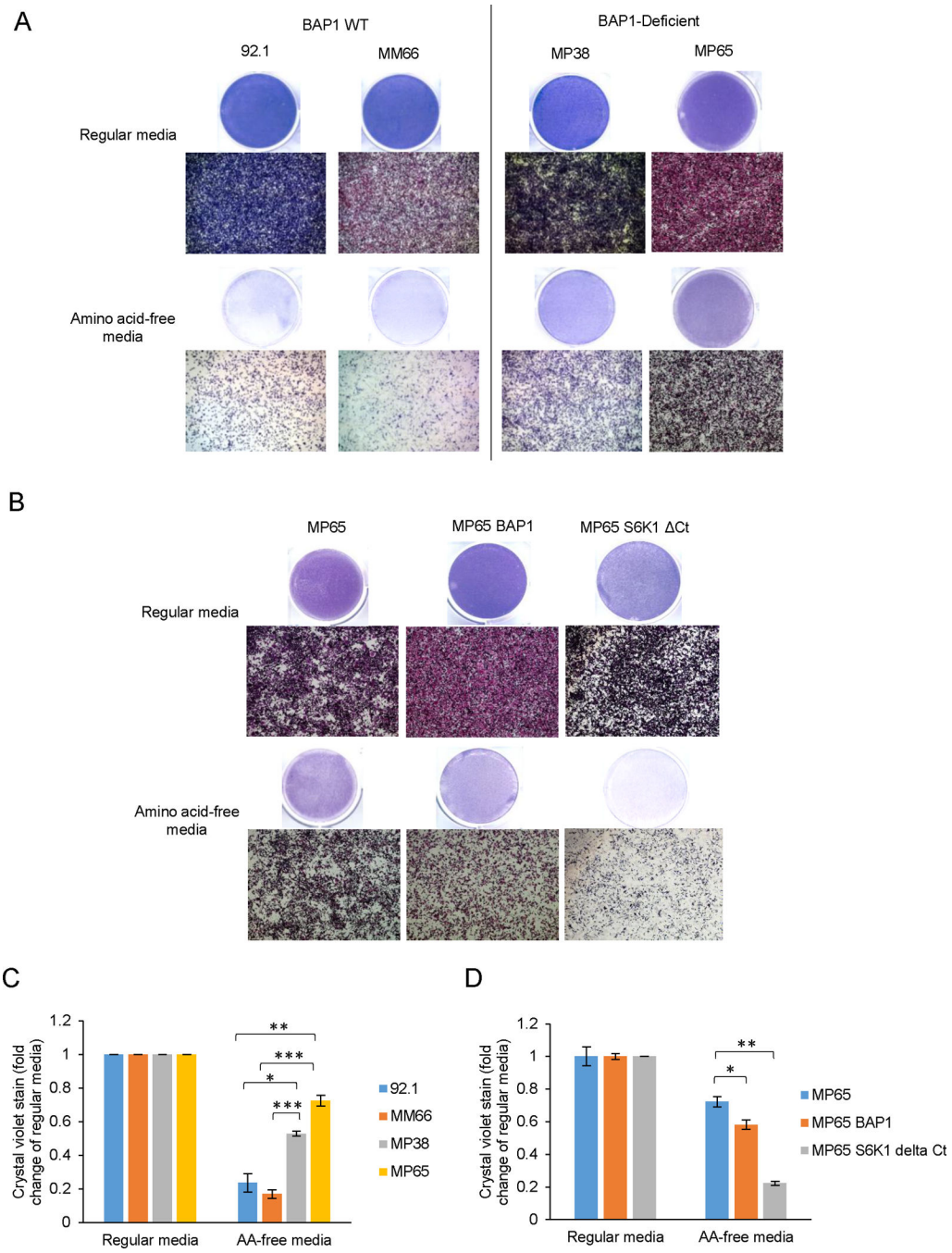

Figure 7: BAP1-deficient cells survive better under amino acid deprivation.

(A) *BAP1* WT (92.1 and MM66) and BAP1-deficient (MP38 and MP65) cells were incubated in amino acid-free (AA-free) culture media for 3 days, and cell viability was detected by crystal violet staining. **(B)** As in (A) in MP65 cells, MP65 cells transfected with BAP1 WT, and MP65 cells transfected with S6K1 ΔCt. **(C and D)** Quantitation of crystal violet staining in (A) and (B), respectively. Data are mean ± S.E.M. from

triplicate experiments (N=3). *p≤0.05, **p≤0.01, ***p≤0.001 by unpaired student's t-test and p-values adjusted using the Hochberg method.